

Rapid Detection of Ag(I) via Size-Induced Photoluminescence Quenching of Biocompatible Green-Emitting, L-Tryptophan-Scaffolded Copper Nanoclusters

Aarya, Telna Thomas, Bibhu Ranjan Sarangi, and Supratik Sen Mojumdar*

Cite This: *ACS Omega* 2023, 8, 14630–14640

Read Online

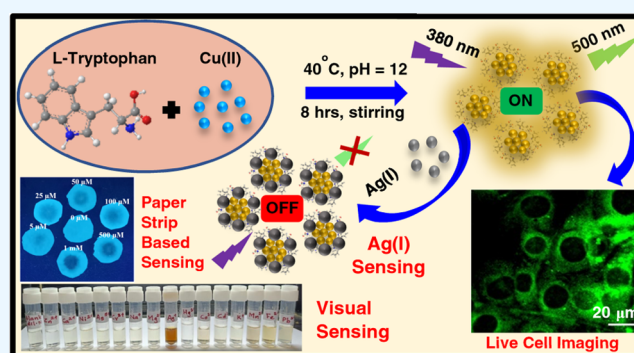
ACCESS |

Metrics & More

Article Recommendations

Supporting Information

ABSTRACT: Atomically precise metal nanoclusters capped with small molecules like amino acids are highly favored due to their specific interactions and easy incorporation into biological systems. However, they are rarely explored due to the challenge of surface functionalization of nanoclusters with small molecules. Herein, we report the synthesis of a green-emitting ($\lambda_{\text{ex}} = 380$ nm, $\lambda_{\text{em}} = 500$ nm), single-amino-acid (L-tryptophan)-scaffolded copper nanocluster (Trp-Cu NC) via a one-pot route under mild reaction conditions. The synthesized nanocluster can be used for the rapid detection of a heavy metal, silver (Ag(I)), in the nanomolar concentration range in real environmental and biological samples. The strong green photoluminescence intensity of the nanocluster quenched significantly upon the addition of Ag(I) due to the formation of bigger nanoparticles, thereby losing its energy quantization. A notable color change from light yellow to reddish-brown can also be observed in the presence of Ag(I), allowing its visual colorimetric detection. Portable paper strips fabricated with the Trp-Cu NC can be reliably used for on-site visual detection of Ag(I) in the micromolar concentration range. The Trp-Cu NC possesses excellent biocompatibility, making it a suitable nanoprobe for cell imaging; thus, it can act as an in vivo biomarker. The nanocluster showed a significant spectral overlap with anticancer drug doxorubicin and thus can be used as an effective fluorescence resonance energy transfer (FRET) pair. FRET results can reveal important information regarding the attachment of the drug to the nanocluster and hence its role as a potential drug carrier for targeted drug delivery within the human body.



1. INTRODUCTION

Ligand-protected noble metal nanoclusters (e.g., Au, Ag, Cu, etc.) emerged as efficient nanoprobess, grabbing considerable recent interest owing to their luminescence properties, ease of synthesis, low cytotoxicity, and high photostability and biocompatibility.^{1–7} These nanoclusters with their improved physicochemical and optical properties have broad applicability in sensing,^{8–13} catalysis,^{3,14} bioimaging,^{9,15} and therapeutics.^{16–18} Metal nanoclusters are ultrasmall particles comprising several to tens of atoms.^{6,19–21} Their extraordinary photophysical properties are associated with the presence of quantized and discrete energy levels due to their small size (<2 nm).^{19–21} Despite the natural abundance, copper nanoclusters have been less explored compared to Au and Ag. Due to its relatively higher oxidation potential, it is challenging to reduce copper, and once formed, the copper nanoclusters can readily undergo oxidative damage.^{21–23}

In protein-capped metal nanoclusters, small amino acids like tryptophan and tyrosine play a crucial role in protecting the nanoclusters by coordinating with the metal core and reducing the metal ions.^{22–25} Thus, one might anticipate that individual amino acids can also play a similar role outside the protein

structure, forming a stable ultrasmall nanocluster without the involvement of a large macromolecule, where the surface properties can be easily tuned. The bidentate carboxylate group and the lone pair of electrons of the amine group of the individual amino acids are promising for protecting the nanocluster, ensuring better metal coordination and specific interaction.⁵ Small-molecule-templated nanoclusters can be easily incorporated within a biological system such as live cells,^{24,26} but surface functionalization of metal nanoclusters with small molecules as capping agents is challenging.²⁴

Tryptophan, one of the eight essential amino acids, is the only precursor for synthesizing melatonin and serotonin. Serotonin is an important neurotransmitter and neuro-modulator responsible for regulating mood, behavior, and cognition, whereas melatonin acts as a regulator of sleep/wake

Received: January 23, 2023

Accepted: April 3, 2023

Published: April 12, 2023



rhythms and reduces oxidative stress.^{27,28} In the liver, tryptophan is converted to niacin (vitamin B3), which has many essential biological functions such as energy metabolism, DNA synthesis, and so on.^{29,30} Tryptophan is primarily found in transmembrane proteins. It helps anchor the membrane proteins with the cell membrane.^{31,32} It has a high affinity to transport across the blood–brain barrier compared to other amino acids³² and thus could act as a potential drug carrier. Although it is found in the lowest concentration in the body, it is a critical component in protein synthesis and essential metabolic pathways.²⁷ Tryptophan-templated copper nanoclusters thus could be a suitable nanoprobe for *in vivo* studies.

Silver, a noble and precious metal, has been extensively used in various fields such as medicines,³³ drug delivery,³⁴ textiles,³⁵ jewelry, catalysis,³⁶ and electronics.³⁷ The antimicrobial property of Ag(I) has been explored in water purification and therapeutic applications.^{33,38} However, the unconstrained release of Ag(I) (a heavy metal) into the environment as a part of many anthropogenic activities and rapid industrial growth has led to a significant increase in its concentration in the environment (especially in water resources), resulting in adverse effects on human health and environment.³⁹ Once it enters the body, it can accumulate and deposit, resulting in many adverse health disorders.^{39,40} Commonly, high concentrations of Ag(I) in the human body can lead to skin discoloration, causing argyria.^{41,42} The interaction of Ag(I) with thiol groups can lead to the inhibition of the enzymatic activity of proteins.^{43,44} Due to its binding affinity toward purine and pyrimidine bases in DNA, silver ions and silver nanoparticles can damage the DNA.⁴⁵ Apart from genotoxicity, it has also been found to induce renal, hepatic, and neurological toxicities.⁴¹ It can displace important metal ions like Ca^{2+} and Zn^{2+} in hydroxyapatite in bone.⁴⁶ Thus, it is essential to detect Ag(I) in biological and environmental systems with high sensitivity and selectivity. However, to date, sensors for rapid and selective detection of Ag(I) ions are limited, with most of the cases involving complex mechanisms or instrumentations.^{47,48} This calls for a simple, reliable, robust, sensitive, water-soluble, biocompatible, cost-effective, time-efficient, and highly selective sensor for the ultrasensitive detection of Ag(I).

Traditionally, available sophisticated analytical techniques commonly used for the detection of Ag(I) involve atomic absorption/emission spectroscopy (AAS/AES),⁴⁹ inductively coupled plasma atomic-emission spectrometry (ICP-AES),⁵⁰ mass spectrometry (ICP-MS),⁵¹ surface-enhanced Raman spectroscopy (SERS),⁵² etc. Even though the detection limits of some of these techniques can reach up to 0.1 nM, they are less favored as they are costly and require cumbersome sample preparation, complicated and sophisticated instrumentation, complex detection process, and trained personnel.⁵³ Fluorescent probes on the other hand are more favored as sensors as they are rapid and user-friendly.^{54,55} Various fluorescent probes have been developed as sensors for Ag(I) using organic templates,⁵⁶ quantum dots,⁵⁷ and nanoparticles.^{43,47,58} The detection methods are rapid and sensitive, but they too suffer from one or more drawbacks; either they are insoluble in water^{59,60} or highly toxic to the human body.⁶¹ Thus, the development of fluorescence-based, biocompatible optical sensors with desirable features is in high demand. Ligand-protected metal nanoclusters thus could be a better choice for the selective detection of Ag(I). Most recently researchers attempted to develop metal nanoclusters for the detection of

Ag(I),^{62–65} but they too need improvements since their limits of detection were high and the cytotoxicity of these nanoclusters was not checked; thus, they could pose a threat to human health.

Here, we report a protocol for the synthesis of a green-emitting, L-tryptophan-stabilized ultrasmall (diameter ~ 2 nm) copper nanocluster (Trp-Cu NC) that can rapidly and selectively detect Ag(I) in the nanomolar concentration range (detection limit ~ 25 nM) in complex systems such as real water samples and human serum. The Trp-Cu NC was found to be highly photostable, highly biocompatible, and have a better quantum yield ($\phi = 0.114$) than the previously reported work.⁶⁶ It has a significant spectral overlap with an anticancer drug (doxorubicin), making it a suitable candidate for a fluorescence resonance energy transfer (FRET) pair to study drug binding/release. The synthesized Trp-Cu NC can be used as a nanoprobe for cell imaging and intracellular studies, making it a suitable candidate for *in vivo* biomarkers. The ability of tryptophan to engage in multiple types of interactions and its role in membrane protein stabilization make the internalization of NC easier for *in vivo* studies, thereby opening up its potential application as a drug carrier.

2. RESULTS AND DISCUSSION

2.1. Green-Emitting Trp-Cu NC. The synthesized tryptophan-stabilized Cu NC showed a strong green photoluminescence intensity ($\lambda_{\text{em}} \sim 500$ nm) with a significant photoluminescence quantum yield (PLQY) ($\phi = 0.114$) when excited at 380 nm, and a 120 nm Stokes shift (Figure 1).

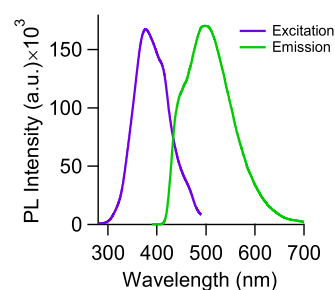


Figure 1. Emission ($\lambda_{\text{ex}} = 380$ nm) and excitation ($\lambda_{\text{em}} = 500$ nm) spectra of Trp-Cu NC.

Compared to the negligible emission intensity of pure tryptophan, the strong photoluminescence intensity of Trp-Cu NC indicated that the luminescent properties are intrinsic to the copper nanocluster and not to the tryptophan scaffold (Figure S1). On mixing L-tryptophan and CuCl_2 solutions, nanocluster formation initiates by the electrostatic interaction between Cu(II) ions and amino and carboxyl groups of tryptophan. Under basic conditions (pH = 12) and in the presence of an external reducing agent, the Cu(II) ions get reduced to Cu(0), forming a nanocluster by coalescence.^{66,67} The zero oxidation state of Cu was confirmed by X-ray photoelectron spectroscopy (XPS) (Figure S2). The peaks at around 932.2 and 952.5 eV correspond to Cu $2p_{3/2}$ and Cu $2p_{1/2}$, respectively, confirming the existence of Cu(0) (Figure S2). Since the difference in binding energies between Cu(0) and Cu(I) is only 0.1 eV, the possibility of the existence of a trace amount of Cu(I) cannot be completely excluded.⁶⁸ However, the absence of a satellite peak at around 942 eV confirms the absence of Cu(II).⁶⁸ The Trp-Cu NC showed

excellent photostability for over 3 weeks when stored at 4 °C under dark conditions (Figure S3). In general, copper nanoclusters are prone to oxidative damage, leading to the quenching of the photoluminescence intensity.^{22,23} However, in the case of Trp-Cu NC, absolutely no quenching of the photoluminescence intensity was observed in the presence of strong oxidizing agents like hydrogen peroxide (H₂O₂) and hypochlorite (ClO⁻), suggesting that the Trp-Cu NC is highly stable against oxidative damage (Figure S4).

The morphology of the nanoclusters was obtained using high-resolution transmission electron microscopy (HRTEM). The TEM image exhibited the existence of monodispersed spherical ultrasmall (average size $\sim 2 \pm 0.1$ nm) Trp-Cu NC (Figure 2). Lattice fringes can also be clearly visible in the

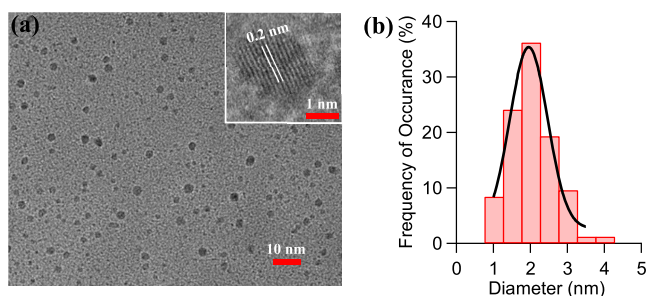


Figure 2. (a) Transmission electron microscopy (TEM) image of Trp-Cu NC confirming the formation of ultrasmall spherical clusters. The lattice fringes are also visible (inset). (b) Size distribution of the nanocluster obtained from the TEM image showing an average size of ~ 2 nm.

TEM image (Figure 2A, inset). The surface charge of the nanoclusters was determined from the zeta potential measurements. For Trp-Cu NC, an average ζ potential was measured to be around -26.3 mV under basic conditions (pH ~ 11.2), suggesting an overall negative surface charge of the nanocluster primarily due to capping agent^{68,69} tryptophan (pI: 5.9) in addition to the cluster. The interaction between the functional groups of tryptophan and copper in the nanocluster was examined using Fourier transform infrared (FTIR) spectroscopy. The FTIR spectra of pure tryptophan and Trp-Cu NC showed a close resemblance (Figure 3a). The bands at around $3000\text{--}3400$ cm⁻¹ correspond to N–H and O–H stretching vibrations. Indole N–H stretching vibration was observed as a distinctive peak at 3394 cm⁻¹. The band at 1660 cm⁻¹ can be assigned to the C=O stretching vibration of an amide bond. A

significant broadening of the bands at around $3000\text{--}3400$ cm⁻¹ was observed in the IR spectra of NC due to Cu–N bond formation.^{67,70} This can be attributed to the efficient stabilization of NC by tryptophan.

The precise chemical composition of Trp-Cu NC was successfully obtained using the mass spectrometry (MALDI–TOF) technique (Figure 3b). By comparing the spectrum of Trp-Cu NC with that of pure tryptophan, we assigned the observed m/z values to corresponding fragments.^{66,71,72} The most dominant base peak centered at $m/z = 401.495$ can be attributed to [Cu₃In + Na⁺]. The next most abundant peaks located at $m/z = 217.674$ and $m/z = 467.469$ can be assigned to the chemical formulas of [CuIn + Na⁺] and [Cu₄In + 3Na⁺], respectively. Some other less intense peaks were also observed, and the respective chemical compositions of these nanoclusters are listed in Table S1.^{66,71,72}

2.2. Selective and Sensitive Detection of Ag(I). The strong photoluminescence intensity of Trp-Cu NC can be completely quenched ($\sim 99\%$) by 500 μM Ag(I) ions (Figure S5). The photoluminescence quantum yield (PLQY) of the Trp-Cu NC decreased from 11.4% in the absence of Ag(I) to zero in the presence of 500 μM Ag(I) ions. Based on this remarkable result, an assay was developed for the rapid detection of Ag(I). A series of metal ions and biomolecules were added to the Trp-Cu NC to check the selectivity of the nanocluster toward Ag(I). Only Ag(I) showed significant quenching of the photoluminescence intensity among all of the screened metal ions and biomolecules (Figure 4). Upon addition of Ag(I) (~ 200 μM), the PL intensity of Trp-Cu NC decreased by ~ 15 -fold ($\sim 93\%$ quenching), while in the presence of other metal ions (~ 500 μM) or common biomolecules present in the human body (such as glucose (~ 5 mM), creatinine (~ 1 mM), tyrosine (~ 1 mM), and dopamine (~ 1 mM)), only a minimal change (≤ 1.5 times decrease) in the PL intensity can be observed, clearly suggesting its selectivity for the detection of Ag(I) (Figure 4). The interference study showed that the presence of other metal ions or biomolecules as interferers in the medium did not affect the selectivity and detection efficiency of the nanocluster toward Ag(I) (Figure S6). Even in the presence of high concentrations (typical concentrations observed in the human body or real samples such as tap water) of other common metal ions (600 μM) or biomolecules (~ 1 mM), on an average ~ 15 -fold quenching of the PL intensity of the nanocluster can be observed by Ag(I) (200 μM), suggesting no significant interference in the selectivity of Ag(I) (Figure S6).

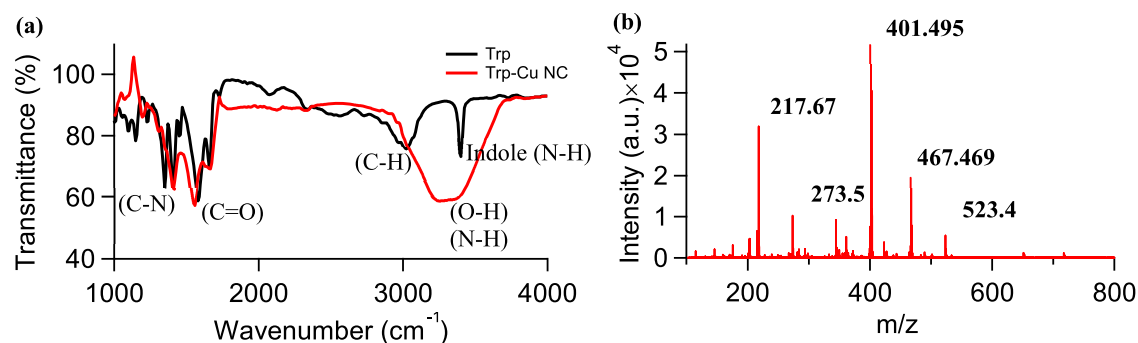


Figure 3. (a) FTIR spectra of tryptophan (black) and Trp-Cu NC (red). (b) Matrix-assisted laser desorption/ionization—time-of-flight (MALDI–TOF) mass spectrum of Trp-Cu NC.

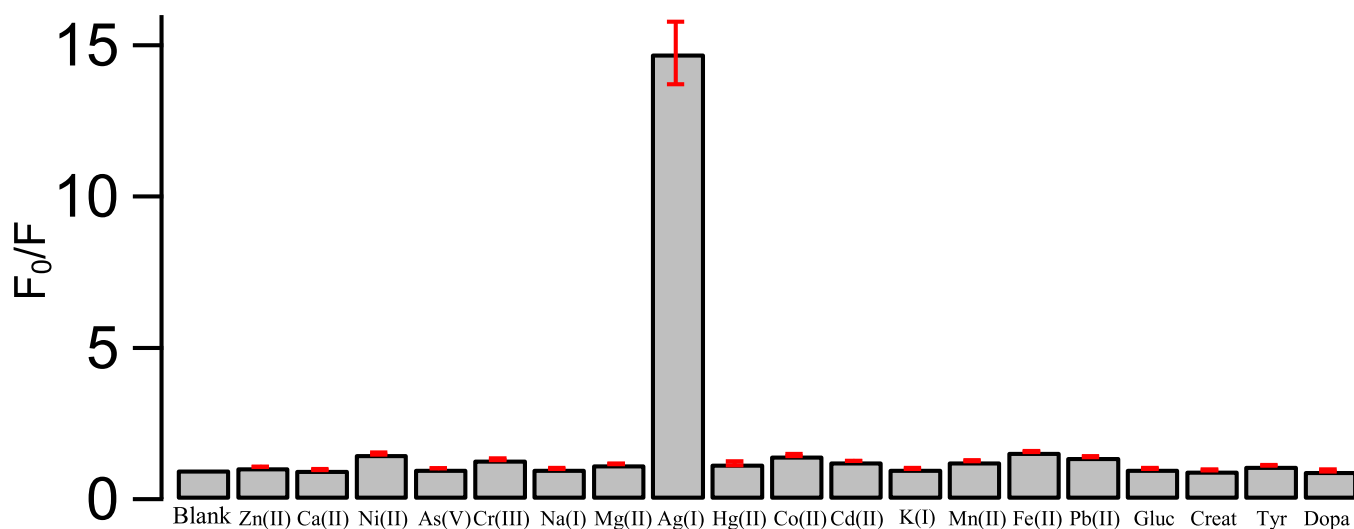


Figure 4. Ratio of the PL intensity ($\lambda_{\text{ex}} = 380 \text{ nm}$, $\lambda_{\text{em}} = 500 \text{ nm}$) of Trp-Cu NC in the absence (F_0) and presence of Ag(I) ($\sim 200 \mu\text{M}$) and different other metal ions ($\sim 500 \mu\text{M}$), or biomolecules (glucose (Gluc) ($\sim 5 \text{ mM}$), creatinine (Creat) ($\sim 1 \text{ mM}$), tyrosine (Tyr) ($\sim 1 \text{ mM}$), and dopamine (Dopa) ($\sim 1 \text{ mM}$)) (F) showing selective detection of Ag(I).



Figure 5. Color change of the diluted nanocluster can be visualized upon the addition of Ag(I) compared to other metal ions ($\sim 500 \mu\text{M}$).

We further investigated the effect of the pH of the medium on the efficiency of the nanocluster toward the detection of Ag(I). The Trp-Cu NC was extremely sensitive in the basic (pH = 11.2) and neutral (pH = 7.4) pH; the PL intensity was readily quenched by ~ 15 -fold upon the addition of Ag(I) ($200 \mu\text{M}$) (Figure S7). However, only 1.2-fold quenching of the PL intensity was observed in the acidic medium (pH = 3.1) on the addition of the same amount of Ag(I) (Figure S7), suggesting that the Trp-Cu NC was extremely effective as an Ag(I) sensor in the basic and neutral pH medium but not in the acidic medium. A significant color change from pale yellow to reddish-brown could also be clearly observed upon the addition of Ag(I) to the nanocluster solutions. This color change was not visible for other metal ions, indicating that the Trp-Cu NC can also be used for visual detection of Ag(I) with utmost selectivity (Figure 5).

Owing to its high reduction potential, Ag(I) can be easily converted to Ag(0) in the presence of any mild reducing agent. Previously, small molecules like tryptophan have been assigned as a reducing agent for the reduction of the metal core during the formation of a stable nanocluster.^{25,66} Thus, upon addition of Ag(I) to the Trp-Cu NC, it can undergo a metallophilic interaction with the Cu core followed by a rapid reduction to Ag(0) by tryptophan and hydrazine present in the system. This reduction process is extremely critical and plays an important role in the sensing mechanism. When treated with HCl or L-cysteine, neither precipitation nor any significant change in the PL intensity was observed, suggesting the presence of Ag(0) in the Trp-Cu NC solution. The zero oxidation state of Ag was further confirmed by XPS studies (Figure S8). Ag(0) was then deposited on the surface of the copper NC, resulting in an

enhancement in the size of the clusters. This increase in the size of Trp-Cu NC after the addition of Ag(I) was confirmed by the TEM image (Figure 6). A significant increase in the size

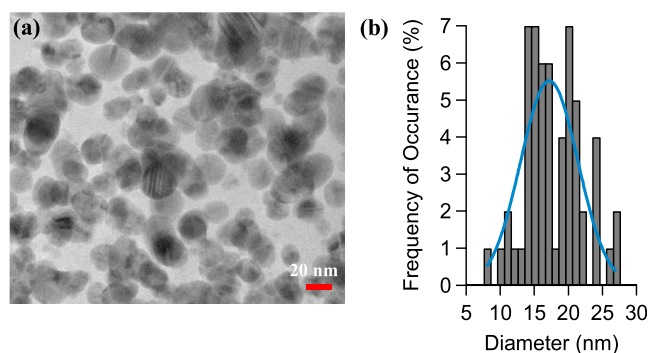


Figure 6. (a) Transmission electron microscopy (TEM) image of Trp-Cu NC in the presence of $500 \mu\text{M}$ Ag(I). (b) Size distribution of the nanocluster in the presence of Ag(I).

from ~ 2 to $\sim 18 \text{ nm}$ (~ 9 fold) was observed from the TEM image, which distinctly indicates the transition from a nanocluster to a nanoparticle. The inherent PL property of Trp-Cu NC due to its quantum size was thus lost due to the formation of nanoparticles. This justifies the drastic reduction in the PL intensity of the NC upon the addition of Ag(I) compared to other metal ions or biomolecules.

The color change from pale yellow to reddish-brown under visible light can also be attributed to the increase in the size of the particles. The reducibility of tryptophan (pI 5.9) and hydrazine drastically decreased in the acidic medium (pH =

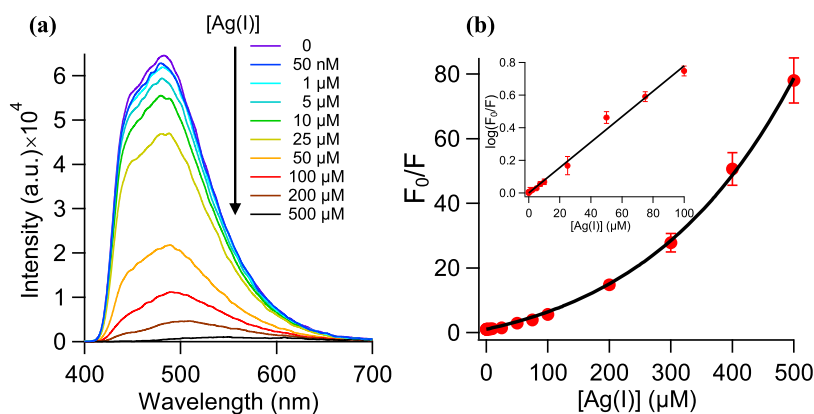


Figure 7. (a) PL intensity of Trp-Cu NC gradually quenched with increasing concentration of Ag(I). (b) Corresponding Stern–Volmer plot showing an upward curvature. The black line represents a fit using eq 1 with both static and dynamic quenching contributions. The inset represents a plot of $\log(F_0/F)$ vs $[Ag(I)]$ (red) with a linear fit (black).

3.1).^{25,73} Thus, the potential reducing agents can no longer reduce Ag(I) to Ag(0) in the acidic medium, thereby decreasing the efficiency of the nanocluster significantly for the detection of Ag(I) in the acidic medium (Figure S7). The FTIR spectra of Trp-Cu NC did not change appreciably upon the addition of Ag(I) (Figure S9). A broad peak at around 3000–3400 cm^{-1} corresponding to N–H and O–H stretching vibrations and a peak at around 1630 cm^{-1} corresponding to the C=O stretching vibration can still be observed (Figure S9). Only the bands resulting from the N–H bending vibration (1400–1570 cm^{-1}) disappeared in the presence of Ag(I), suggesting that the scaffold conformation becomes stiffer in the presence of Ag(I).

The sensitivity of the Trp-Cu NC was examined by gradually adding Ag(I) to the nanocluster solution. With increasing concentration of Ag(I) (from the nanomolar (~ 25 nM) to micromolar (~ 500 μM) concentration range), the photoluminescence intensity of the nanocluster gradually decreased and completely quenched ($\sim 99\%$) at around ~ 500 μM Ag(I) concentration (Figure 7a). Interestingly, when F_0/F (where F_0 and F are the PL intensities in the absence and presence of Ag(I), respectively) was plotted as a function of Ag(I) concentration (intensity-based Stern–Volmer Plot), a non-linear curve with an upward curvature was observed (Figure 7b), which is a typical characteristic of a combination of static and dynamic quenching mechanisms.^{74,75} This plot can be nicely fitted to the following equation containing both the static and dynamic contributions: $\frac{F_0}{F} = (1 + K[Q])e^{V[Q]}$, where $[Q]$ is the concentration of the quencher and K and V are the dynamic and static quenching constants, respectively.^{74,75} Thus, the dynamic and static quenching constants ($K = 3.9 \times 10^4 \text{ M}^{-1}$, $V = 2.7 \times 10^3 \text{ M}^{-1}$) can be obtained readily from the fitted curve. In our study, the dynamic quenching constant (K) appeared to be an order of magnitude faster than the static quenching constant (V). The size of the complex in the presence of Ag(I) can be estimated from the static quenching constant.^{75–77} Static quenching can usually be explained in terms of a “sphere of action” within which the probability of quenching is unity. The volume of this sphere can be estimated from $v = 1000V/N_A$, where V is the static quenching constant and N_A is the Avogadro number.^{75–77} In the present study, $V = 2.7 \times 10^3 \text{ M}^{-1}$ corresponds to a volume of $44.8 \times 10^{-19} \text{ cm}^3$, which leads to a sphere with an average diameter of ~ 20 nm, consistent

with the average size of 18 nm obtained from the TEM study. When $\log(F_0/F)$ is plotted against $[Ag(I)]$, a linear fit can be obtained in the concentration range from 0 to 100 μM (Figure 7b, inset), which can be further used as a calibration curve ($\log(F_0/F) = 7.8 \times 10^3[Q]$) for the estimation of Ag(I) in real complex systems. The limit of detection (LOD) for Ag(I) was estimated to be 25 nM (please refer to Note 1 of the Supporting Information), which is either comparable to or better than other sensors for the detection of Ag(I) (Table S2). Our detection limit is well below the permissible amount of silver in the human body and the maximum limit to be present in the drinking water (0.05 mg L^{-1} , i.e., 0.463 μM) determined by the World Health Organization (WHO).⁶³

The lifetime-based quenching process is effective in determining the quenching mechanism. Quenching of PL lifetime can only occur due to dynamic/collisional quenching.^{75,78} The average lifetime of Trp-Cu NC in the absence of any quencher was observed to be 5.2 ns (Figure S10a and Table S3). Upon gradual addition of Ag(I), no significant change in the average lifetime was observed, suggesting predominantly a static quenching mechanism (Figure S10b and Table S3), thus only partially agreeing with the results obtained from the intensity-based Stern–Volmer plot. However, upon careful examination, a slight but subtle quenching effect can be seen in the ultrafast time scale (considering only the average of τ_1 and τ_2 from Table S3, the average ultrafast component slightly decreased from 730 ps in the absence of Ag(I) to 660 ps in the presence of 400 μM Ag(I)), suggesting the possibility of a swift dynamic quenching process (Figure S10c) that could have been better resolved with a higher-time-resolution instrument.

We have further extended these sensing studies to develop a simple paper strip-based sensor for rapid visual detection of Ag(I). The paper strips (Whatman filter paper) were cut into desired shapes, immersed in Trp-Cu NC, and air-dried at room temperature. When kept under UV light, the strips showed a cyan PL intensity (Figure S11). On addition of different concentrations of Ag(I) (~ 10 μL), a dark spot appeared at the center of the paper strip due to the quenching of the PL intensity. This dark spot intensified with increasing concentration of Ag(I). By analyzing the brightness of these images, the results can be further quantified.⁷⁹ Thus, Trp-Cu NC can be used as a simple, portable, cost-effective, paper strip-based sensor for the rapid quantitative detection of Ag(I) in the micromolar concentration range.

2.3. Quantification of Ag(I) in Complex Samples. To check the applicability and reliability of our sensor in detecting Ag(I) in real-life complex systems, we have chosen tap water and human blood serum as environmentally and biologically relevant samples, respectively. Typically, the reliability of a sensor is determined by spiking a real sample with a known amount of the analyte and subsequently calculating its recovery. In our study, we also followed a similar method to check the reliability of the sensor. Initially, no Ag(I) was detected in the tap water and the human blood serum. We spiked the complex systems with a known amount of Ag(I) and subsequently estimated the amount of Ag(I) in the samples experimentally using the Trp-Cu NC (Table 1). The

Table 1. Recovery of Ag(I) from Different Complex Systems

sample	concentration of Ag(I) added (μM)	concentration of Ag(I) recovered (μM) (mean \pm s.e.m.) ($n = 3$)	RSD (%) ($n = 3$)	concentration of Ag(I) obtained from the ICP-OES method (μM)
tap water	0.5	0.55 ± 0.2	59.5	0.76
	50	57.36 ± 12	36.2	49.56
	100	85.6 ± 4	8.1	94.65
human blood serum	0.5	0.59 ± 0.1	36.3	0.61
	50	53.22 ± 6	19.5	51.9
	100	89.86 ± 4	7.7	104.49

values listed in Table 1 suggest that we can estimate and recover the amount of Ag(I) in these complex systems with more than 90% accuracy on average using the Trp-Cu NC. The experimentally obtained results using the synthesized nanocluster as a sensor matched nicely with the values obtained from a standard method using the ICP-OES technique (Table 1). The results thus demonstrate that our sensor can be used for rapid and reliable detection of Ag(I) in complex environmentally and biologically relevant samples in the presence of other interferers and analytes.

2.4. Cell Viability and Imaging. The *in vitro* toxicity study of the Trp-Cu NC showed excellent biocompatibility over a wide range of concentrations (Figure 8a). The cells were significantly viable ($\sim 40 \pm 8\%$) even at a high concentration ($\sim 16 \mu\text{g mL}^{-1}$) of the nanocluster (Figure 8a), suggesting that the nanocluster is nontoxic and can be used as a biomarker for intracellular studies. The IC_{50} value for the nanocluster was measured to be $\sim 11 \mu\text{g mL}^{-1}$. The high quantum yield, high photostability, and noncytotoxicity make the Trp-Cu NC a suitable nanoprobe for cell imaging studies. Upon incubation

of the nanocluster with 3T3 cells, high-resolution bright PL images of the cell can be obtained under a 405 nm excitation laser using a confocal microscope (Figure 8b), suggesting that the synthesized nanocluster can be used for live-cell imaging. Figure 8b indicates that the nanocluster is preferentially localized in the cytosolic region of the cell. The internalization of the nanocluster within the cell takes place through endocytosis, which is a fundamental process of internalizing molecules through the cell membrane.³⁰ Hypothetically, small scaffolds (e.g., amino acids) should easily penetrate the cell membrane compared to their bigger counterparts (e.g., proteins);²⁶ this is exactly what we observed in this study. Compared to Lys-Cu NC,⁷⁸ the L-tryptophan-scaffolded nanocluster could easily pass through the cell membrane, making it a better nanoprobe for cell imaging and other *in vivo* studies. Apart from size, better penetration may be explained by the fact that tryptophan can easily attach to the cell membrane,^{31,32} thereby making the endocytosis process easier.

2.5. Trp-Cu NC: A Suitable FRET Pair for an Anticancer Drug. Fluorescence resonance energy transfer (FRET) is an efficient nonradiative energy transfer technique to estimate the distance between two fluorophores (donor and acceptor) in the nanometer range ($<10 \text{ nm}$).^{75,81,82} FRET efficiency is extremely sensitive to the distance between the donor and acceptor and can be easily calculated from the relative fluorescence intensities of the donor in the absence and presence of the acceptor.^{75,81,82} FRET has been widely used for the study of protein folding,⁸³ DNA and RNA detection,^{84,85} interactions of a small molecule with an assembly,^{22,86} etc. FRET experiments critically depend upon the availability of a suitable FRET pair where the donor emission significantly overlaps with the acceptor absorption.^{75,81,82}

Finding a biocompatible FRET pair for an anticancer drug that can map the *in vivo* targeted drug release is extremely challenging. The synthesized Trp-Cu NC showed significant spectral overlap with anticancer drug doxorubicin (dox) (Figure 9a) and thus can be used as an effective FRET pair, where the nanocluster can act as a donor, while the anticancer drug can be used as an acceptor. The Förster distance (R_0) was calculated to be 3.2 nm, lying within the acceptable range for an ideal FRET pair.⁷⁵ Upon the addition of doxorubicin to the nanocluster, a significant quenching of the photoluminescence intensity of the nanocluster was observed followed by a concomitant increase in the emission intensity of doxorubicin, suggesting effective FRET between the NC and doxorubicin (Figure 9b). The corresponding FRET efficiency was

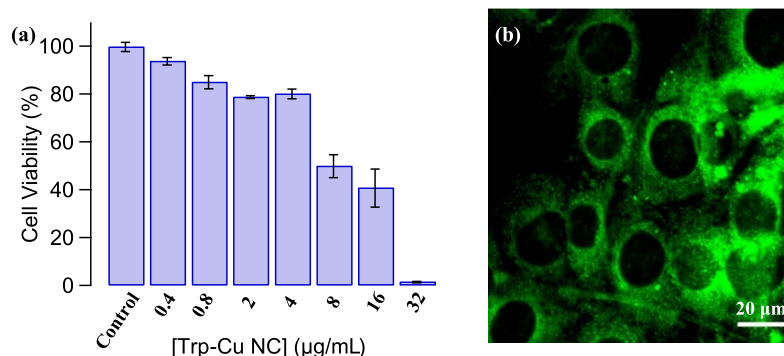


Figure 8. (a) Cell viability assay showing that the nanocluster is not cytotoxic to the 3T3 cells (errors represent standard errors on mean with $n = 3$). (b) Confocal microscopy image of 3T3 cells incubated with Trp-Cu NC ($\lambda_{\text{ex}} = 405 \text{ nm}$).

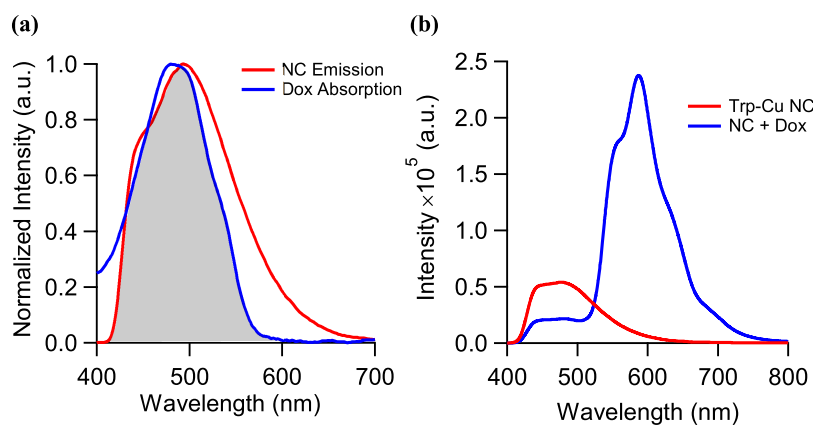
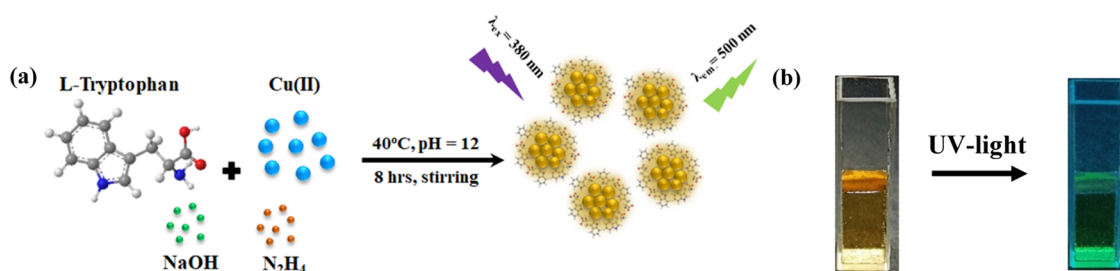


Figure 9. (a) Spectral overlap between normalized emission spectra ($\lambda_{\text{ex}} = 380$ nm) of the Trp-Cu nanocluster (donor) (red) and the absorption spectra of doxorubicin (acceptor) (blue). (b) Emission spectra ($\lambda_{\text{ex}} = 380$ nm) of the Trp-Cu nanocluster (donor) in the absence (red) and presence of 100 μM doxorubicin (acceptor) (blue).

Scheme 1. (a) Schematic Representation of Synthesis of Trp-Cu NC; (b) Trp-Cu NC under Visible Light (Yellowish-Brown) and Ultra-Violet (UV) Light (Green)



calculated to be $\sim 60\%$ with an intermolecular distance of ~ 2.98 nm between the donor and acceptor. FRET experiments thus can shed important light on the binding and release of the anticancer drug in vivo, thereby opening up the possibility of using the nanocluster as a potent nanodrug carrier for localized and controlled drug release in cancer patients.

3. CONCLUSIONS

We have developed a simple one-pot protocol for the synthesis of an ultrasmall, photoluminescent, and water-soluble L-tryptophan-scaffolded copper nanocluster. The synthesized nanocluster with strong green photoluminescence intensity and high quantum yield exhibited drastic quenching of the PL intensity in the presence of Ag(I). Thus, a turn-off PL assay was developed for rapid, selective, and sensitive detection of Ag(I) in the nanomolar concentration range. The quenching of the PL intensity of the nanocluster by Ag(I) can be attributed to the conversion of atomically precise nanoclusters to nanoparticles, thereby losing its energy quantization. The quenching mechanism can be explained by both static and dynamic processes as indicated by the PL intensity-based Stern–Volmer plot, partially agreeing with the lifetime data. On-site visual detection of Ag(I) was also achieved with portable paper strips coated with Trp-Cu NC. The excellent biocompatibility of the nanocluster was confirmed by cell viability studies. Small tryptophan molecules as a scaffold allowed the nanocluster to easily penetrate the cell membrane; thus, it was successfully used as a biomarker for live-cell imaging, making it a promising candidate for in vivo studies as an intracellular sensor. Significant spectral overlap with an anticancer drug (doxorubicin) allows it to be used as a FRET

pair adding further value to its features. Overall, the synthesized Trp-Cu NC can be used as an excellent nanosensor for Ag(I) detection, bioimaging, in vivo studies and can also be potentially extended for various theragnostic applications.

4. MATERIALS AND METHODS

4.1. Materials. L-tryptophan was purchased from Sisco Research Laboratories Pvt., Ltd. (SRL). Copper chloride ($\text{CuCl}_2 \cdot 2\text{H}_2\text{O}$), sodium hydroxide (NaOH), and hydrazine hydrate ($\text{N}_2\text{H}_4 \cdot \text{H}_2\text{O}$) used for the synthesis of Trp-Cu NC were purchased from Nice Chemicals (NICE). The following metal salts for examining metal ion sensing of NC were purchased either from SRL or NICE: mercuric chloride (HgCl_2), silver nitrate (AgNO_3), calcium chloride (CaCl_2), sodium chloride (NaCl), magnesium chloride (MgCl_2), manganese chloride (MnCl_2), nickel sulfate (NiSO_4), cadmium chloride (CdCl_2), chromic nitrate [$\text{Cr}(\text{NO}_3)_2$], ferrous chloride (FeCl_2), lead nitrate [$\text{Pb}(\text{NO}_3)_2$], cobalt nitrate [$\text{Co}(\text{NO}_3)_2$], zinc sulfate (ZnSO_4), sodium arsenate (Na_2HASO_4), and nickel sulfate (NiSO_4). Hydrogen peroxide (H_2O_2), creatinine, sodium hypochlorite (NaOCl) solution, and concentrated hydrochloric acid (HCl) were purchased from NICE. L-Cysteine and L-tyrosine were purchased from SRL. Quinine hemi-sulfate dye, human serum, glucose, and dopamine hydrochloride were purchased from Sigma-Aldrich. Doxorubicin hydrochloride for FRET studies was purchased from Tokyo Chemical Industry (TCI). Doubly distilled water from the Biopak Polisher Milli-Q water system (CDUFB1001) was used for preparing all the solutions. All the reagents were used as received without any further purification.

4.2. Synthesis of L-Tryptophan-Scaffolded Copper Nanocluster. To synthesize L-tryptophan-scaffolded copper nanocluster (Trp-Cu NC), 1 mL of 0.15 mM CuCl₂ was added to 2 mL of 7.5 mM L-tryptophan solution in a 1:100 (Cu/Trp) molar ratio. The reaction mixture was vigorously stirred at 40 °C for half an hour. This was followed by dropwise addition of 100 μL of 1 M NaOH to adjust the pH of the solution to 12. After half an hour of stirring, 50 μL of 80% hydrazine hydrate was added dropwise to the reaction mixture. The solution was then kept for vigorous stirring at 40 °C for 8 h (Scheme 1a). The formation of NC was indicated by the appearance of a yellowish-brown transparent solution that turned green under UV light (Scheme 1b). After completion of the reaction, the sample was stored at 4 °C under dark conditions for further use.

4.3. Instrumentation. Steady-state fluorescence measurements were performed using a PerkinElmer Fluorescence Spectrometer (FL 8500). The L-tryptophan-scaffolded Cu NC solution was excited at 380 nm, and the spectra were scanned from 390 to 700 nm at a scan speed of 240 nm min⁻¹, keeping excitation and emission slit widths at 5 nm with a 430 nm emission filter. Lifetime measurements were done on a time-correlated single photon counting setup (LifeSpec-II, Edinburgh Instruments, U.K.) using a 375 nm pulsed diode laser with an instrument response function of 150 ps. The size of the NC was determined using high-resolution transmission electron microscopy (HRTEM) from JEOL, Japan (model no. JEM-2100 Plus). The sample was drop-cast on a carbon-coated copper grid. Fourier transform infrared (FTIR) spectra was recorded using an IR Tracer-100 FTIR spectrophotometer from Shimadzu Scientific Instruments scanning in the wavenumber range of 7800–350 cm⁻¹ at 0.2 cm⁻¹ resolution. For matrix-assisted laser desorption/ionization—time-of-flight (MALDI–TOF) mass spectrometry analysis, a Bruker made Ultraflex extreme MALDI–TOF analyzer was used with trans-2-[3-(4-*tert*-Butylphenyl)-2-methyl-2-propenyldiene]-malononitrile (DCTB) as the matrix. ζ potential was measured using Zetasizer Nano-ZS from Malvern Panalytical. XPS measurements were done on an ESCA Omicron nanotechnology (Oxford Instruments, Germany) spectrometer with Mg Kα and Al Kα as the X-ray source. Inductively coupled plasma-optical emission spectrometry (ICP-OES) measurements were done using a PerkinElmer Optima 5300 DV instrument for the quantitative determination of Ag(I) in real samples. The photoluminescence quantum yield (ϕ) of the nanocluster was measured using the method reported earlier.⁷⁸

4.4. Metal-Sensing Studies. For the metal-sensing studies, the diluted solution of Trp-Cu NC (~25 times) was incubated with the desired concentration of different metal cations (Cd(II), Cr(III), Fe(II), Ni(II), Co(II), Zn(II), Hg(II), As(V), Mn(II), Na(I), K(I), Ca(II), Mg(II), Pb(II), and Ag(I)) and biomolecules (glucose, creatinine, tyrosine, and dopamine) for ~3 min prior to the measurement. For the interference study, the desired concentration of interferers was added to the Trp-Cu NC and the PL intensities were recorded and marked as the intensity without Ag(I) (*F*₀). About 200 μM Ag(I) was then added to the resulting mixture and incubated for ~5 min followed by the PL intensity measurement (*F*). Nitrate salt of the metal ions was used for the interference study to avoid precipitation of Ag(I). To test the sensitivity, increasing concentrations of Ag(I) (25 nM to 500 μM) were added to 1 mL of diluted NC and emission spectra were

recorded after 3 min of incubation after each addition. Reported errors represent the standard error of the mean (s.e.m.) calculated from at least three or more independent measurements (*n* ≥ 3).

4.5. Fluorometric Analysis of Ag(I) with Trp-Cu NC-Coated Paper Strips. The Whatman filter paper was cut into pieces in a circular shape and immersed into Trp-Cu NC solution. After 10 min, it was removed and air-dried at room temperature. Ten microliters of different concentrations of Ag(I) (5, 25, 50, 100, 500, and 1000 μM) was then drop-cast on the paper strips coated with NC and observed under a UV lamp.

4.6. Detection of Ag(I) in Real Samples. The prepared NC was applied to estimate Ag(I) in real specimens like tap water and human serum. Various concentrations of Ag(I) (0.5, 50, and 100 μM) were spiked into 1 mL of NC solution containing 100 μL of real specimens. After 3 min of incubation, the emission spectra were recorded. Errors represent the standard error of the mean (s.e.m.) calculated from three independent measurements (*n* = 3).

4.7. Cell Viability and Imaging. The cell viability studies were done following the MTT-based assay mentioned earlier.⁷⁸ Briefly, the 3T3 (normal mouse fibroblast) cells were incubated with varying concentrations (0.4–32 μg mL⁻¹) of Trp-Cu NC for 24 h. After incubation, MTT was added to each well (final concentration ~0.5 mg mL⁻¹). The resulting formazan crystals were dissolved in dimethyl sulfoxide (DMSO) and absorbance was recorded in a plate reader (Biotech Epoch 2NS Gen5) at 590 nm using a 620 nm reference filter. Normalized viability and s.e.m. were calculated from at least three independent measurements done for each concentration. For imaging, the cells were incubated with 8 μg mL⁻¹ (~20 μM) Trp-Cu NC for 6 h. Postincubation cells were fixed using paraformaldehyde. Imaging was done using a confocal microscope (Olympus FLUOVIEW FV3000) with suitable excitation (λ_{ex} = 405 nm) and emission parameters.

4.8. Fluorescence Resonance Energy Transfer (FRET). The FRET efficiency (*E*_{FRET}) can be calculated using the following equation⁷⁵

$$E_{\text{FRET}} = 1 - \frac{I_{\text{DA}}}{I_{\text{D}}} \quad (1)$$

where *I*_{DA} and *I*_D are the photoluminescence intensities of the donor in the presence and absence of the acceptor, respectively. The Förster distance (*R*₀) was estimated from the spectral overlap *J*(λ) using the following equation⁷⁵

$$R_0 = 0.211[\kappa^2 n^{-4} Q_{\text{D}} J(\lambda)]^{1/6} \quad (2)$$

where κ² is the orientation factor (normally assumed as 2/3 for random orientation), *n* is the refractive index, and *Q*_D is the quantum yield. The overlap integral *J*(λ) can be measured from the equation below

$$J(\lambda) = \frac{\int_0^\infty I_{\text{D}}(\lambda) \epsilon_{\text{A}}(\lambda) \lambda^4 d\lambda}{\int_0^\infty I_{\text{D}}(\lambda) d\lambda} \quad (3)$$

■ ASSOCIATED CONTENT

Supporting Information

The Supporting Information is available free of charge at <https://pubs.acs.org/doi/10.1021/acsomega.3c00462>.

Emission spectra, photostability of the NC, effect of oxidizing agents, pH effect on Ag(I) sensitivity, interference study, XPS data, TCSPC data, paper strip image, and comparison with other Ag(I) sensors (PDF)

AUTHOR INFORMATION

Corresponding Author

Supratik Sen Mojumdar – Department of Chemistry, Indian Institute of Technology Palakkad, Palakkad 678 557 Kerala, India; orcid.org/0000-0002-2552-1350;
Email: supratik@iitpkd.ac.in

Authors

Aarya – Department of Chemistry, Indian Institute of Technology Palakkad, Palakkad 678 557 Kerala, India
Telna Thomas – Department of Chemistry, Indian Institute of Technology Palakkad, Palakkad 678 557 Kerala, India
Bibhu Ranjan Sarangi – Department of Physics and Department of Biological Sciences and Engineering, Indian Institute of Technology Palakkad, Palakkad 678 557 Kerala, India

Complete contact information is available at:

<https://pubs.acs.org/10.1021/acsomega.3c00462>

Notes

The authors declare no competing financial interest.

ACKNOWLEDGMENTS

S.S.M. thanks SERB, Government of India (Project no. SRG/2020/001710) and IIT Palakkad for financial assistance. B.R.S. thanks SERB, Government of India (Project no. ECR/2016/001986) for financial support. Aarya thanks UGC, Government of India, and T.T. thanks SERB, Government of India (Project no. SRG/2020/001710) for providing fellowships. S.S.M. thanks the Central Instrumentation Facility (CIF), IIT Palakkad for FTIR measurements, Dr. Pratik Sen, IIT Kanpur for lifetime measurements, and SCIF SRM Institute of Science and Technology for TEM measurements.

REFERENCES

- (1) Lu, Y.; Chen, W. Sub-Nanometre Sized Metal Clusters: From Synthetic Challenges to the Unique Property Discoveries. *Chem. Soc. Rev.* **2012**, *41*, 3594–3623.
- (2) Baghdasaryan, A.; Bürgi, T. Copper Nanoclusters: Designed Synthesis, Structural Diversity, and Multiplatform Applications. *Nanoscale* **2021**, *13*, 6283–6340.
- (3) Meng, X.; Zare, I.; Yan, X.; Fan, K. Protein-protected Metal Nanoclusters: An Emerging Ultra-small Nanozyme. *Wiley Interdiscip. Rev.: Nanomed. Nanobiotechnol.* **2020**, *12*, No. e1602.
- (4) Lin, Z.; Goswami, N.; Xue, T.; Chai, O. J. H.; Xu, H.; Liu, Y.; Su, Y.; Xie, J. Engineering Metal Nanoclusters for Targeted Therapeutics: From Targeting Strategies to Therapeutic Applications. *Adv. Funct. Mater.* **2021**, *31*, No. 2105662.
- (5) Liu, W.; Wang, J.; Yuan, S.; Chen, X.; Wang, Q. Chiral Superatomic Nanoclusters Ag₄₇ Induced by the Ligation of Amino Acids. *Angew. Chem., Int. Ed.* **2021**, *60*, 11430–11435.
- (6) Xie, J.; Zheng, Y.; Ying, J. Y. Protein-Directed Synthesis of Highly Fluorescent Gold Nanoclusters. *J. Am. Chem. Soc.* **2009**, *131*, 888–889.
- (7) Xavier, P. L.; Chaudhari, K.; Baksi, A.; Pradeep, T. Protein-Protected Luminescent Noble Metal Quantum Clusters: An Emerging Trend in Atomic Cluster Nanoscience. *Nano Rev.* **2012**, *3*, No. 14767.
- (8) Rajamanikandan, R.; Ilanchelian, M. Red Emitting Human Serum Albumin Templated Copper Nanoclusters as Effective Candidates for Highly Specific Biosensing of Bilirubin. *Mater. Sci. Eng. C* **2019**, *98*, 1064–1072.
- (9) Krishna Kumar, A. S.; Tseng, W.-L. Perspective on Recent Developments of near Infrared-Emitting Gold Nanoclusters: Applications in Sensing and Bio-Imaging. *Anal. Methods* **2020**, *12*, 1809–1826.
- (10) Zheng, S.; Yin, H.; Li, Y.; Bi, F.; Gan, F. One-Step Synthesis of L-Tryptophan-Stabilized Dual-Emission Fluorescent Gold Nanoclusters and Its Application for Fe³⁺ Sensing. *Sens. Actuators, B* **2017**, *242*, 469–475.
- (11) Shellaiah, M.; Sun, K. W. Luminescent Metal Nanoclusters for Potential Chemosensor Applications. *Chemosensors* **2017**, *5*, No. 36.
- (12) Shellaiah, M.; Simon, T.; Thirumalaivasan, N.; Sun, K. W.; Ko, F.-H.; Wu, S.-P. Cysteamine-Capped Gold-Copper Nanoclusters for Fluorometric Determination and Imaging of Chromium(VI) and Dopamine. *Microchim. Acta* **2019**, *186*, No. 788.
- (13) Lettieri, M.; Palladino, P.; Scarano, S.; Minunni, M. Copper Nanoclusters and Their Application for Innovative Fluorescent Detection Strategies: An Overview. *Sens. Actuators Rep.* **2022**, *4*, No. 100108.
- (14) Wen, F.; Dong, Y.; Feng, L.; Wang, S.; Zhang, S.; Zhang, X. Horseradish Peroxidase Functionalized Fluorescent Gold Nanoclusters for Hydrogen Peroxide Sensing. *Anal. Chem.* **2011**, *83*, 1193–1196.
- (15) Ramadurai, M.; Rajendran, G.; Bama, T. S.; Prabhu, P.; Kathiravan, K. Biocompatible Thiolate Protected Copper Nanoclusters for an Efficient Imaging of Lung Cancer Cells. *J. Photochem. Photobiol. B* **2020**, *205*, No. 111845.
- (16) Shahsavari, S.; Hadian-Ghazvini, S.; Hooriabad Saboor, F.; Menbari Oskouie, I.; Hasany, M.; Simchi, A.; Rogach, A. L. Ligand Functionalized Copper Nanoclusters for Versatile Applications in Catalysis, Sensing, Bioimaging, and Optoelectronics. *Mater. Chem. Front.* **2019**, *3*, 2326–2356.
- (17) Zare, I.; Chevrier, D. M.; Cifuentes-Rius, A.; Moradi, N.; Xianyu, Y.; Ghosh, S.; Trapiella-Alfonso, L.; Tian, Y.; Shourangiz-Haghighi, A.; Mukherjee, S.; Fan, K.; Hamblin, M. R. Protein-Protected Metal Nanoclusters as Diagnostic and Therapeutic Platforms for Biomedical Applications. *Mater. Today* **2021**, DOI: 10.1016/j.mattod.2020.10.027.
- (18) Lai, W.-F.; Wong, W.-T.; Rogach, A. L. Development of Copper Nanoclusters for In Vitro and In Vivo Theranostic Applications. *Adv. Mater.* **2020**, *32*, No. 1906872.
- (19) Benavides, J.; Quijada-Garrido, I.; García, O. The Synthesis of Switch-off Fluorescent Water-Stable Copper Nanocluster Hg²⁺ Sensors via a Simple One-Pot Approach by an *in Situ* Metal Reduction Strategy in the Presence of a Thiolated Polymer Ligand Template. *Nanoscale* **2020**, *12*, 944–955.
- (20) Song, X.-R.; Goswami, N.; Yang, H.-H.; Xie, J. Functionalization of Metal Nanoclusters for Biomedical Applications. *Analyst* **2016**, *141*, 3126–3140.
- (21) Bhattacharyya, K.; Mukherjee, S. Fluorescent Metal Nanoclusters as Next Generation Fluorescent Probes for Cell Imaging and Drug Delivery. *Bull. Chem. Soc. Jpn.* **2018**, *91*, 447–454.
- (22) Ghosh, S.; Das, N. K.; Anand, U.; Mukherjee, S. Photostable Copper Nanoclusters: Compatible Förster Resonance Energy-Transfer Assays and a Nanothermometer. *J. Phys. Chem. Lett.* **2015**, *6*, 1293–1298.
- (23) Akhuli, A.; Preeyanka, N.; Chakraborty, D.; Sarkar, M. Turn-Off Detection of Reactive Oxidative Species and Turn-On Detection of Antioxidants Using Fluorescent Copper Nanoclusters. *ACS Appl. Nano Mater.* **2022**, *5*, 5826–5837.
- (24) Chakraborty, S.; Mukherjee, S. Role of Small Moiety of a Large Ligand: Tyrosine Templated Copper Nanoclusters. *J. Phys. Chem. Lett.* **2021**, *12*, 3266–3273.
- (25) Saleh, S. M.; El-Sayed, W. A.; El-Manawaty, M. A.; Gassoumi, M.; Ali, R. Microwave-Assisted Rapid Synthesis of Luminescent Tryptophan-Stabilized Silver Nanoclusters for Ultra-Sensitive Detection of Fe(III), and Their Application in a Test Strip. *Biosensors* **2022**, *12*, No. 425.

- (26) Mosquera, J.; García, I.; Liz-Marzán, L. M. Cellular Uptake of Nanoparticles versus Small Molecules: A Matter of Size. *Acc. Chem. Res.* **2018**, *51*, 2305–2313.
- (27) Richard, D. M.; Dawes, M. A.; Mathias, C. W.; Acheson, A.; Hill-Kapturczak, N.; Dougherty, D. M. L-Tryptophan: Basic Metabolic Functions, Behavioral Research and Therapeutic Indications. *Int. J. Tryptophan Res.* **2009**, *2*, 45–60.
- (28) Paredes, S. D.; Barriga, C.; Reiter, R. J.; Rodríguez, A. B. Assessment of the Potential Role of Tryptophan as the Precursor of Serotonin and Melatonin for the Aged Sleep-Wake Cycle and Immune Function: *Streptopelia Risoria* as a Model. *Int. J. Tryptophan Res.* **2009**, *2*, 23–36.
- (29) Fukuwatari, T.; Shibata, K. Nutritional Aspect of Tryptophan Metabolism. *Int. J. Tryptophan Res.* **2013**, *6*, 3–8.
- (30) Gasperi, V.; Sibilano, M.; Savini, I.; Catani, M. V. Niacin in the Central Nervous System: An Update of Biological Aspects and Clinical Applications. *Int. J. Mol. Sci.* **2019**, *20*, No. 974.
- (31) de Jesus, A. J.; Allen, T. W. The Role of Tryptophan Side Chains in Membrane Protein Anchoring and Hydrophobic Mismatch. *Biochim. Biophys. Acta, Biomembr.* **2013**, *1828*, 864–876.
- (32) Khemaissa, S.; Sagan, S.; Walrant, A. Tryptophan, an Amino-Acid Endowed with Unique Properties and Its Many Roles in Membrane Proteins. *Crystals* **2021**, *11*, No. 1032.
- (33) Sim, W.; Barnard, R.; Blaskovich, M. A. T.; Ziora, Z. Antimicrobial Silver in Medicinal and Consumer Applications: A Patent Review of the Past Decade (2007–2017). *Antibiotics* **2018**, *7*, No. 93.
- (34) Prasher, P.; Sharma, M.; Mudila, H.; Gupta, G.; Sharma, A. K.; Kumar, D.; Bakshi, H. A.; Negi, P.; Kapoor, D. N.; Chellappan, D. K.; Tambuwala, M. M.; Dua, K. Emerging Trends in Clinical Implications of Bio-Conjugated Silver Nanoparticles in Drug Delivery. *Colloid Interface Sci. Commun.* **2020**, *35*, No. 100244.
- (35) Windler, L.; Height, M.; Nowack, B. Comparative Evaluation of Antimicrobials for Textile Applications. *Environ. Int.* **2013**, *53*, 62–73.
- (36) Sharma, R. K.; Yadav, S.; Dutta, S.; Kale, H. B.; Warkad, I. R.; Zbořil, R.; Varma, R. S.; Gawande, M. B. Silver Nanomaterials: Synthesis and (Electro/Photo) Catalytic Applications. *Chem. Soc. Rev.* **2021**, *50*, 11293–11380.
- (37) Chen, D.; Qiao, X.; Qiu, X.; Chen, J. Synthesis and Electrical Properties of Uniform Silver Nanoparticles for Electronic Applications. *J. Mater. Sci.* **2009**, *44*, 1076–1081.
- (38) Mijndendonckx, K.; Leys, N.; Mahillon, J.; Silver, S.; Van Houdt, R. Antimicrobial Silver: Uses, Toxicity and Potential for Resistance. *BioMetals* **2013**, *26*, 609–621.
- (39) Ratte, H. T. Bioaccumulation and Toxicity of Silver Compounds: A Review. *Environ. Toxicol. Chem.* **1999**, *18*, 89–108.
- (40) Lansdown, A. B. G. A Pharmacological and Toxicological Profile of Silver as an Antimicrobial Agent in Medical Devices. *Adv. Pharmacol. Sci.* **2010**, *2010*, 1–16.
- (41) Hadrup, N.; Sharma, A. K.; Loeschner, K. Toxicity of Silver Ions, Metallic Silver, and Silver Nanoparticle Materials after in Vivo Dermal and Mucosal Surface Exposure: A Review. *Regul. Toxicol. Pharmacol.* **2018**, *98*, 257–267.
- (42) Mota, L.; Dinis-Oliveira, R. J. Clinical and Forensic Aspects of the Different Subtypes of Argyria. *J. Clin. Med.* **2021**, *10*, No. 2086.
- (43) Huy, G. D.; Zhang, M.; Zuo, P.; Ye, B.-C. Multiplexed Analysis of Silver(i) and Mercury(ii) Ions Using Oligonucleotide–Metal Nanoparticle Conjugates. *Analyst* **2011**, *136*, 3289–3294.
- (44) Gordon, O.; Vig Slenters, T.; Brunetto, P. S.; Villaruz, A. E.; Sturdevant, D. E.; Otto, M.; Landmann, R.; Fromm, K. M. Silver Coordination Polymers for Prevention of Implant Infection: Thiol Interaction, Impact on Respiratory Chain Enzymes, and Hydroxyl Radical Induction. *Antimicrob. Agents Chemother.* **2010**, *54*, 4208–4218.
- (45) Jiravova, J.; Tomankova, K. B.; Harvanova, M.; Malina, L.; Malohlava, J.; Luhova, L.; Panacek, A.; Manisova, B.; Kolarova, H. The Effect of Silver Nanoparticles and Silver Ions on Mammalian and Plant Cells in Vitro. *Food Chem. Toxicol.* **2016**, *96*, 50–61.
- (46) Arulraj, A. D.; Devasenathipathy, R.; Chen, S.-M.; Vasantha, V. S.; Wang, S.-F. Highly Selective and Sensitive Fluorescent Chemosensor for Femtomolar Detection of Silver Ion in Aqueous Medium. *Sens. Bio-Sens. Res.* **2015**, *6*, 19–24.
- (47) Li, B.; Du, Y.; Dong, S. DNA Based Gold Nanoparticles Colorimetric Sensors for Sensitive and Selective Detection of Ag(I) Ions. *Anal. Chim. Acta* **2009**, *644*, 78–82.
- (48) Dalmieda, J.; Zubiarrain-Laserna, A.; Ganepola, D.; Selvaganapathy, P. R.; Kruse, P. Chemiresistive Detection of Silver Ions in Aqueous Media. *Sens. Actuators, B* **2021**, *328*, No. 129023.
- (49) Mohammadi, S. Z.; Afzali, D.; Heshmati, Z. Ligand-Less *In Situ* Surfactant-Based Solid Phase Extraction for Preconcentration of Silver from Natural Water Samples Prior to Its Determination by Atomic Absorption Spectroscopy. *Toxicol. Environ. Chem.* **2013**, *95*, 1299–1308.
- (50) Poitras, E. P.; Levine, M. A.; Harrington, J. M.; Essader, A. S.; Fennell, T. R.; Snyder, R. W.; Black, S. L.; Sumner, S. S.; Levine, K. E. Development of an Analytical Method for Assessment of Silver Nanoparticle Content in Biological Matrices by Inductively Coupled Plasma Mass Spectrometry. *Biol. Trace Elem. Res.* **2015**, *163*, 184–192.
- (51) Clark, N. J.; Clough, R.; Boyle, D.; Handy, R. D. Development of a Suitable Detection Method for Silver Nanoparticles in Fish Tissue Using Single Particle ICP-MS. *Environ. Sci. Nano* **2019**, *6*, 3388–3400.
- (52) Guo, H.; Xing, B.; Hamlet, L. C.; Chica, A.; He, L. Surface-Enhanced Raman Scattering Detection of Silver Nanoparticles in Environmental and Biological Samples. *Sci. Total Environ.* **2016**, *554*–555, 246–252.
- (53) Zhou, M.; Lin, T.; Gan, X. Colorimetric Aggregation Assay for Silver(I) Based on the Use of Aptamer Modified Gold Nanoparticles and C-Ag(I)-C Interaction. *Microchim. Acta* **2017**, *184*, 4671–4677.
- (54) Carter, K. P.; Young, A. M.; Palmer, A. E. Fluorescent Sensors for Measuring Metal Ions in Living Systems. *Chem. Rev.* **2014**, *114*, 4564–4601.
- (55) Li, L.; Wang, J.; Xu, S.; Li, C.; Dong, B. Recent Progress in Fluorescent Probes For Metal Ion Detection. *Front. Chem.* **2022**, *10*, No. 875241.
- (56) Liu, Y.; Liu, Y.; Li, Z.; Liu, J.; Xu, L.; Liu, X. An Unusual Red-to-Brown Colorimetric Sensing Method for Ultrasensitive Silver(I) Ion Detection Based on a Non-Aggregation of Hyperbranched Polyethylenimine Derivative Stabilized Gold Nanoparticles. *Analyst* **2015**, *140*, 5335–5343.
- (57) Liao, S.; Zhao, X.; Zhu, F.; Chen, M.; Wu, Z.; Song, X.; Yang, H.; Chen, X. Novel S, N-Doped Carbon Quantum Dot-Based “off-on” Fluorescent Sensor for Silver Ion and Cysteine. *Talanta* **2018**, *180*, 300–308.
- (58) Wang, F.; Lu, Y.; Chen, Y.; Sun, J.; Liu, Y. Colorimetric Nanosensor Based on the Aggregation of AuNP Triggered by Carbon Quantum Dots for Detection of Ag⁺ Ions. *ACS Sustainable Chem. Eng.* **2018**, *6*, 3706–3713.
- (59) Cui, W.; Wang, L.; Xiang, G.; Zhou, L.; An, X.; Cao, D. A Colorimetric and Fluorescence “Turn-off” Chemosensor for the Detection of Silver Ion Based on a Conjugated Polymer Containing 2,3-Di(Pyridin-2-Yl)Quinoxaline. *Sens. Actuators, B* **2015**, *207*, 281–290.
- (60) Kang, J.; Choi, M.; Kwon, J. Y.; Lee, E. Y.; Yoon, J. New Fluorescent Chemosensors for Silver Ion. *J. Org. Chem.* **2002**, *67*, 4384–4386.
- (61) Shiohara, A.; Hoshino, A.; Hanaki, K.-I.; Suzuki, K.; Yamamoto, K. On the Cyto-Toxicity Caused by Quantum Dots. *Microbiol. Immunol.* **2004**, *48*, 669–675.
- (62) Hu, Y.-L.; Liu, A.-Y.; Wu, B.-C.; Zhao, R.-X.; Pu, Z.-F.; Ling, J.; Cao, Q. Modulating Fluorescence Emission of L-Methionine-Stabilized Au Nanoclusters from Green to Red and Its Application for Visual Detection of Silver Ion. *Microchem. J.* **2021**, *166*, No. 106198.
- (63) Kang, J.; Gao, P.; Zhang, G.; Shi, L.; Zhou, Y.; Wu, J.; Shuang, S.; Zhang, Y. Rapid Sonochemical Synthesis of Copper Nanoclusters

with Red Fluorescence for Highly Sensitive Detection of Silver Ions. *Microchem. J.* **2022**, *178*, No. 107370.

(64) An, M.; Li, H.; Su, M.; Wang, M. C.; Shen, S. G.; Gao, Z. F.; Dong, J. X. Cu²⁺ Enhanced Fluorescent Ag Nanoclusters with Tunable Emission from Red to Yellow and the Application for Ag⁺ Sensing. *Spectrochim. Acta, Part A* **2021**, *252*, No. 119484.

(65) Wang, J.; Liu, A.-Y.; Wu, B.-C.; Wen, Q.-L.; Pu, Z.-F.; Zhao, R.-X.; Ling, J.; Cao, Q. Highly Selective and Rapid Detection of Silver Ions by Using a “Turn on” Non-Fluorescent Cysteine Stabilized Gold Nanocluster Probe. *Anal. Methods* **2021**, *13*, 2099–2106.

(66) Kardar, Z. S.; Shemirani, F.; Zadmand, R. Determination of Iron(II) and Iron(III) via Static Quenching of the Fluorescence of Tryptophan-Protected Copper Nanoclusters. *Microchim. Acta* **2020**, *187*, No. 81.

(67) Anusuyadevi, K.; Wu, S. P.; Velmathi, S. Reversible Enhancement of Fluorescence in Acidic PH Driven by Tryptophan Stabilized Copper Nanoclusters and Its Application in Bioimaging. *J. Photochem. Photobiol. Chem.* **2021**, *421*, No. 113526.

(68) Ghosh, R.; Sahoo, A. K.; Ghosh, S. S.; Paul, A.; Chattopadhyay, A. Blue-Emitting Copper Nanoclusters Synthesized in the Presence of Lysozyme as Candidates for Cell Labeling. *ACS Appl. Mater. Interfaces* **2014**, *6*, 3822–3828.

(69) Zhou, T.; Huang, Y.; Li, W.; Cai, Z.; Luo, F.; Yang, C. J.; Chen, X. Facile Synthesis of Red-Emitting Lysozyme-Stabilized Ag Nanoclusters. *Nanoscale* **2012**, *4*, 5312–5315.

(70) Zhao, X.; Zhao, R. G.; Yang, W. S. Self-Assembly of L-Tryptophan on the Cu(001) Surface. *Langmuir* **2002**, *18*, 433–438.

(71) Zhang, P.; Chan, W.; Ang, I. L.; Wei, R.; Lam, M. M. T.; Lei, K. M. K.; Poon, T. C. W. Revisiting Fragmentation Reactions of Protonated α -Amino Acids by High-Resolution Electrospray Ionization Tandem Mass Spectrometry with Collision-Induced Dissociation. *Sci. Rep.* **2019**, *9*, No. 6453.

(72) Domingues, M. R. M.; Domingues, P.; Reis, A.; Fonseca, C.; Amado, F. M. L.; Ferrer-Correia, A. J. V. Identification of Oxidation Products and Free Radicals of Tryptophan by Mass Spectrometry. *J. Am. Soc. Mass Spectrom.* **2003**, *14*, 406–416.

(73) Miao, R.; Compton, R. G. The Electro-Oxidation of Hydrazine: A Self-Inhibiting Reaction. *J. Phys. Chem. Lett.* **2021**, *12*, 1601–1605.

(74) Mátyus, L.; Szöllösi, J.; Jenei, A. Steady-State Fluorescence Quenching Applications for Studying Protein Structure and Dynamics. *J. Photochem. Photobiol. B* **2006**, *83*, 223–236.

(75) *Principles of Fluorescence Spectroscopy*; Lakowicz, J. R., Ed.; Springer <https://www.springer.com/gp/book/9780387312781> (accessed April 17, 2020).

(76) Eftink, M. R.; Ghiron, C. A. Fluorescence Quenching of Indole and Model Micelle Systems. *J. Phys. Chem. A* **1976**, *80*, 486–493.

(77) Casali, E.; Petra, P. H.; Ross, J. B. A. Fluorescence Investigation of the Sex Steroid Binding Protein of Rabbit Serum: Steroid Binding and Subunit Dissociation. *Biochemistry* **1990**, *29*, 9334–9343.

(78) Sebastian, A.; Aarya, Sarangi, B. R.; Sen Mojumdar, S. Lysozyme Protected Copper Nano-Cluster: A Photo-Switch for the Selective Sensing of Fe²⁺. *J. Photochem. Photobiol. Chem.* **2023**, *436*, No. 114378.

(79) Wang, C.-M.; Chen, C.-Y.; Liao, W.-S. Paper-Polymer Composite Devices with Minimal Fluorescence Background. *Anal. Chim. Acta* **2017**, *963*, 93–98.

(80) Doherty, G. J.; McMahon, H. T. Mechanisms of Endocytosis. *Annu. Rev. Biochem.* **2009**, *78*, 857–902.

(81) Ha, T. Single-Molecule Fluorescence Resonance Energy Transfer. *Methods* **2001**, *25*, 78–86.

(82) Stryer, L. Fluorescence Energy Transfer as a Spectroscopic Ruler. *Annu. Rev. Biochem.* **1978**, *47*, 819–846.

(83) Schuler, B.; Eaton, W. A. Protein Folding Studied by Single-Molecule FRET. *Curr. Opin. Struct. Biol.* **2008**, *18*, 16–26.

(84) Dey, D.; Saha, J.; Roy, A. D.; Bhattacharjee, D.; Sinha, S.; Paul, P. K.; Chakraborty, S.; Hussain, S. A. Sensing of DNA Conformation Based on Change in FRET Efficiency between Laser Dyes. *Sens. Actuators, B* **2014**, *204*, 746–753.

(85) Wijesinghe, K. M.; Kanak, M. A.; Harrell, J. C.; Dhakal, S. Single-Molecule Sensor for High-Confidence Detection of MiRNA. *ACS Sens.* **2022**, *7*, 1086–1094.

(86) Xiao, Y.; Shu, F.; Wong, K.-Y.; Liu, Z. Förster Resonance Energy Transfer-Based Biosensing Platform with Ultrasmall Silver Nanoclusters as Energy Acceptors. *Anal. Chem.* **2013**, *85*, 8493–8497.